RESEARCH ARTICLE | AUGUST 07 2024

# Improving pulsed laser induced fluorescence distribution function analysis through matched filter signal processing

T. J. Gilbert ; T. E. Steinberger ; E. E. Scime



*Rev. Sci. Instrum.* 95, 083521 (2024)
https://doi.org/10.1063/5.0215510

Review of Scientific Instruments ARTICLE pubs.aip.org/aip/rsi

# Improving pulsed laser induced fluorescence distribution function analysis through matched filter signal processing

Cite as: Rev. Sci. Instrum. 95, 083521 (2024); doi: 10.1063/5.0215510
Submitted: 24 April 2024 • Accepted: 19 July 2024 •
Published Online: 7 August 2024



T. J. Gilbert,[a] T. E. Steinberger, and E. E. Scime

## AFFILIATIONS

Department of Physics and Astronomy, West Virginia University, P.O. Box 6315, Morgantown, West Virginia 26506, USA

[a]Author to whom correspondence should be addressed: tyler.j.gilbert@outlook

## ABSTRACT

Laser induced fluorescence is used to measure argon ion heating during magnetic reconnection in the PHase Space MApping experiment (PHASMA). Sufficient signal-to-noise ratio (SNR) of the processed signal with pulsed laser injection is a delicate balance between saturation of the absorption line and injecting enough laser power to overcome the spontaneous emission of the plasma at the fluorescence wavelength. Averaging over many laser pulses and integrating over the fluorescence lifetime improves the SNR of the processed signal (processed SNR) when the SNR of the laser pulse time series is small (pulse SNR), but for laser powers small enough to avoid saturation, averaging over hundreds of pulses is needed to obtain an appreciable processed SNR over the entire Doppler-broadened absorption line. Here, we describe a matched filter processing method that significantly improves the SNR of the final measurement with fewer shots averaged. Investigation of simulated measurements validated by experimental results suggests that the matched filter method provides up to a 20% improvement in the processed SNR, resulting in less uncertainty in distribution function fits.





## I. INTRODUCTION

In recent studies in the PHAse Space MApping (PHASMA) experiment, electron velocity distribution functions (VDFs) have been successfully measured during magnetic reconnection with Thomson scattering using a high-power pulsed laser.[1,2] Based on the mass of the ions used in PHASMA (argon), the scale size of the current sheet that forms during reconnection, and the strength of the background (guide) magnetic field, theory predicts that the magnetic reconnection is controlled entirely by the electron dynamics, i.e., it is electron-only reconnection.[3] However, the fraction of magnetic energy that heats or energizes ions (if any)[4] has not been directly measured during electron-only reconnection in PHASMA. Laser induced fluorescence (LIF) is a valuable tool for measuring the distribution functions of ions and neutral atoms without the use of perturbative probes and is routinely used in laboratory plasmas to measure ion heating.[5] Implementation of LIF during magnetic reconnection experiments in PHASMA has been plagued with poor signal-to-noise ratio (SNR) and saturation challenges.

In velocity-resolved LIF in plasmas, light from the decay of an excited electronic state (excited by laser pumping, typically from a metastable or ground state) is recorded as a function of laser wavelength to measure the VDF of the target species. The LIF emission intensity is often very small compared to spontaneous emission from the plasma at the same wavelength. To accomplish LIF in steady-state plasma, modulation of a continuous wave (CW) laser and lock-in amplification techniques are used to increase the SNR by orders of magnitude. However, magnetic reconnection experiments in PHASMA employ a plasma gun that pulses on a time scale of tens of microseconds and emits a bright broadband flash of light. The light emitted during the plasma gun discharge is so intense that even with fast modulation and a high-frequency lock-in amplifier, the fluorescence of a focused CW laser is too low intensity to achieve a detectable LIF signal. Pulsed lasers deliver orders of magnitude more photons over a shorter period of time to the plasma than CW lasers. When used for LIF in PHASMA, the result is a pulse of fluorescent emission that is detectable through simple emission signal averaging (sometimes even in a single emission measurement).

While pulsed LIF overcomes the background light issue in our pulsed plasma, it introduces other complications. First, excessive laser energy results in significant power broadening (line saturation) of the measured VDF. Since a key measurement is the width of

the absorption line, i.e., the plasma temperature, pulsed LIF results in artificially large temperature measurements. Reducing power broadening by using smaller laser pulse energies also reduces the processed SNR, potentially making the signal undetectable. Second, the repetition rate of the laser (a 10 Hz ns laser) is too small to perform multiple LIF measurements during a single plasma gun pulse. Therefore, measuring the time-resolved velocity distribution requires many measurements at a single laser wavelength at a single time in the plasma gun pulse, then shifting to a new wavelength and repeating the averaged measurement. With enough averaged measurements at a range of discrete laser wavelengths, the particle VDF is obtained. However, the entire process must then be repeated at a different time in the plasma pulse to study the evolution of the particle VDF during the plasma gun pulse. LIF measurements then require hundreds of plasma gun pulses and are extraordinarily time consuming for a plasma gun cadence of one pulse per 30 s.

Matched filter analysis has been used in a variety of fields, e.g., telecommunications, radar, and the detection of gravitational waves, to greatly enhance the processed SNR of time series measurements.[6] Given a known template present in a signal with additive stochastic noise, matched filter analysis yields remarkable improvements in detection thresholds and SNR. Here, we show how applying matched filter analysis to pulsed LIF time series measurements improves the processed SNR of velocity-resolved distribution function measurements, facilitating the detection of LIF signals with less pulse averaging at low energies.

## II. BACKGROUND

### A. Matched filter theory

Common methods for LIF signal analysis from pulsed laser injection rely on the extraction of the peak of the fluorescent signal measured with a photomultiplier tube (PMT) or integrating the PMT signal over an optimal time interval based on the decay time of the emission and the time response of the PMT.[7] The peak detection method fails for small pulse SNR values.[7] In the case of small pulse SNR, both peak detection and pulse integration also require averaging over many identical pulses to obtain viable levels of signal. Matched filter analysis is now the gold-standard for the extraction of pulsed signals from small pulse SNR time-series measurements.

Matched filter analysis cross correlates a noisy measured signal with a known reference signal to maximize the processed SNR by convolving the measured signal with the time-reversed conjugated reference signal. A critical factor in matched filter analysis is the requirement of a known reference signal. In the analysis presented in this work, all signals are real, and no conjugation is necessary.

As shown in Fig. 1, a large pulse SNR PMT signal due to the fluorescence from a single laser pulse is well modeled by the pulse fit equation[8]

$$R(t) = B + A\left(1 - \exp\left(-\frac{t-t_0}{\tau_1}\right)\right)^m \exp\left(-\frac{t-t_0}{\tau_2}\right)H(t-t_0). \quad (1)$$

The parameter $\tau_1$ determines the rise time of the pulse and depends on the temporal pulse width of the laser. The parameter $\tau_2$ determines the decay time of the fluorescent pulse and depends on the lifetime of the excited transition state, including all processes that depopulate the upper state, e.g., spontaneous decay of the upper state and state quenching collisions. $A$ is the amplitude of the pulse, and $m$ affects the rate of the rise of the pulse and shifts the location of the signal peak relative to time $t = 0$. A $t - t_0$ shift may also be used in conjunction with the Heaviside step function $H(t - t_0)$ to shift the location of the pulse without altering the rise of the pulse. In Fig. 1, $t = 0$ for the model pulse signal equation is referenced to ~20 ns before the laser pulse occurs. $B$ is any DC offset in the measured signal due to the steady-state background noise level. Parameters $\tau_1$, $\tau_2$, $m$, and $A$ are the constants for a given laser and excitation-decay sequence when the plasma conditions are held fixed. Once these parameters have been determined from measurements of pulses with a large SNR, the signal line shape is known and serves as the reference signal to then be used in a matched filter analysis for measuring distribution functions in a similar plasma with the same laser.

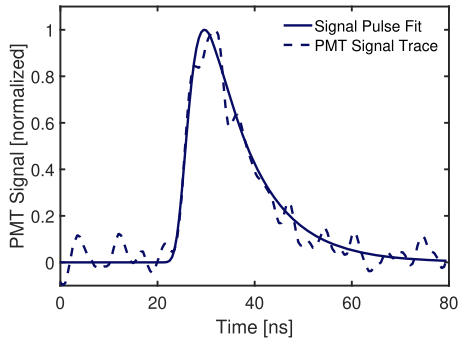


**FIG. 1.** An example PMT trace (dashed) of the fluorescent signal generated by the LIF pulse. The measurement is fit by Eq. (1) (solid). This example time series is one of the measurements described in Sec. IV.

The matched filter analysis process[9] begins with a measured signal $M(t)$ over a time interval $t_1 \le t \le t_2$ at discrete time steps spaced by $\Delta t$ and a reference signal $R(t)$ over the time interval $t_1 + T \le t \le t_2 + T$ using the same discrete time step $\Delta t$. $T$ is a time offset that is chosen to ensure the reference signal pulse fits within the measurement time interval. The measured and reference signals (measured at discrete time steps) are indexed with an integer $n$ such that $M(t) = M(n)$ and $R(t + T) = R(n)$, where $n$ is an integer in the range $0 \le n \le N - 1$, and $N = (t_2 - t_1)/\Delta t$.

The matched filter output $S(x)$, where $x$ is an integer in the range $1 \le x \le 2N - 1$, is the convolution of the measured signal and the reversed reference signal $R(x - n)$ summed over all elements of $n$,

$$S(x) = \sum_{n=0}^{N-1} R(x-n)M(n). \quad (2)$$

The maximum value of $S(x)$ is the strength of the LIF signal embedded in the time series at that laser wavelength. The maximum occurs at a time of $N + L$, where $L$ is the offset, in time steps, between the reference signal and the measured signal. The time offset between the measured and reference signals is determined by defining $S(N)$ as $t = 0$, with $(x - N)\Delta t$ defining a new x-axis. Shown in Fig. 2 is an

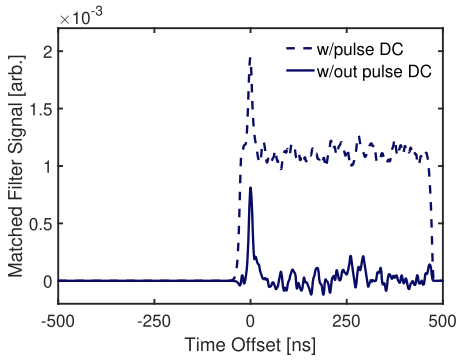


**FIG. 2.** Matched filter analysis of pulses such as those shown in Fig. 1. A DC offset of the pulse results in a DC offset of the output (dashed). The peak location is determined by the offset between the PMT signal pulse and the reference pulse.

example of Eq. (2) using the measured LIF signal from PHASMA and the model reference signal (as shown in Fig. 1) plotted as a function of the time offset. If the maximum occurs at $L = 0$, the reference and measured signals are perfectly aligned. Changes in $L$ provide a measure of drift in the timing of the LIF signal.

### B. Laser induced fluorescence

For this work, electrons are excited from an argon ion metastable state to an excited state that has a large branching ratio to a different energy state than the original metastable state, i.e., a three-level LIF scheme. Random thermal motion and bulk flow of the ions result in a Doppler shift of the absorption frequency. By scanning a narrow linewidth laser over a range of frequencies around the rest frame absorption frequency $\nu_o$ and measuring the resulting fluorescent intensity, the absorption line shape is measured. For narrow linewidth lasers and ideal measurement conditions, the line shape measurement is a direct measurement of the Doppler broadened velocity distribution. In the case of large laser linewidths or saturation broadening, the measured linewidth is corrected to obtain the true Doppler broadened distribution,[10]

$$I(\nu) = \alpha + \beta \exp\left(-\frac{(\nu - \nu_o - \nu_D)^2}{2\sigma^2}\right). \tag{3}$$

$I(\nu)$ is the intensity of the fluorescent signal as a function of the laser frequency $\nu$, $\alpha$ is the background intensity, $\beta$ is the maximum signal amplitude, $\nu_o$ is the rest frame frequency of the transition, and $\nu_D$ is the mean frequency of the fit to the absorbed photons relative to the rest frame frequency of the transition. The drift velocity of the bulk population is obtained from $\nu_D = U_D\nu_o/c$, where $U_D$ is the drift velocity and $c$ is the speed of light. The temperature is derived from the standard deviation $\sigma = \sqrt{k_B T\nu_o^2/mc^2}$, where $k_B$ is the Boltzmann constant, $T$ is the temperature, and $m$ is the mass of the atom or ion.

In CW LIF, the laser output is typically modulated with a mechanical chopper or an acousto-optic modulator, and the laser frequency is scanned across the entire absorption line. The signal collected from a wavelength-filtered PMT (filtered at the emission wavelength) is fed into a lock-in amplifier that references the modulation frequency to isolate the fluorescent signal from the background.[11] In pulsed LIF, the laser is stepped through discrete wavelengths along the absorption line, and the time series of the fluorescent emission is recorded directly from the filtered PMT for each pulse of the laser. Multiple PMT traces are typically averaged together to improve the pulse SNR at each wavelength.

The pulsed laser used in this experiment has a linewidth comparable to the Doppler broadened absorption line shape and, therefore, the laser linewidth cannot be neglected in the analysis. Thus, each LIF measurement is fit to a Voigt profile, a convolution of the Doppler Gaussian distribution function line shape from Eq. (3), and a Lorentzian laser line shape. A Voigt profile is described by

$$V(\nu;\sigma,\gamma) = \alpha + \beta Re\left(w\left[\frac{(\nu - \nu_D) + i\gamma}{\sqrt{2}\sigma}\right]\right), \tag{4}$$

where $V(\nu;\ \sigma,\gamma)$ is the intensity of the fluorescent signal, with $\sigma$ and $\gamma$ being the Gaussian standard deviation and Lorentzian half-width at half-maximum of the laser, respectively. $w[z]$ is the Faddeeva function that is estimated to have an accuracy of $10^{-13}$ by a MATLAB function from Abrarov and Quine.[12] With a known laser half-width half-maximum (HWHM), the Faddeeva function is evaluated as a function of $\sigma$ and $\nu_D$, enabling the determination of the bulk drift velocity and temperature from fits of Eq. (4) to the measurements. Using a Voigt profile instead of a purely Maxwellian profile becomes more important as the temperature decreases.

Saturation of the absorption line also contributes to the artificial broadening of the measured absorption line shape. The LIF signal increases linearly with laser intensity until the ions can no longer absorb additional photons (all the ions have been excited out of their metastable state, and the LIF signal no longer increases with laser intensity). Deviation from the expected linear dependence is often used as a metric to infer laser saturation, although when performing pulsed laser experiments, saturation can have nebulous definitions. For reliable results, it is best to perform measurements using laser energies in the linear regime of signal vs laser energy. Intense lasers may also result in the stimulated emission of the excited state back to the targeted state, causing additional broadening. For the pulsed measurements presented here, classical saturation is unlikely to occur since the time the laser pumps the target state (~6 ns) is much less than the lifetime (spontaneous emission) of the excited state (~40 ns), and equilibrium between pumping, stimulated emission, and spontaneous emission is not established.[13]

Even in the absence of classical laser saturation, with the finite width of the laser line at large laser intensities (i.e., the spectral wings of the laser line shape), a strong fluorescence signal is observed even when the central laser frequency is not tuned to the absorption line. Goeckner *et al.* showed that for pulsed LIF measurements in argon ions, laser broadening effects appear as an additional, wide background feature overlaid on the unsaturated central peak of the velocity distribution.[14]

## III. DATA SIMULATION

### A. Methodology

To highlight the differences between the matched filter and integration techniques, we begin with artificially generated VDFs

obeying a Voigt profile. The parameters of the VDF [as described by Eq. (3)] are chosen to best match the experimental parameters. The VDF consists of twenty evenly spaced wavelengths, shifted by random Gaussian noise based on the observed standard deviation of the laser wavelength, with three points of background in each wing of the distribution. A series of reference pulses [as described by Eq. (1)] are generated for each wavelength with parameters typical of ion LIF (see Sec. IV for additional details). The signal amplitudes are set by the value of the ideal distribution at that wavelength and multiplied by a random Gaussian factor to represent the energy variation of the pulsed laser. One of several different types of noise is added to each pulse based on a chosen pulse SNR, defined as the maximum pulse amplitude for the entire distribution divided by the standard deviation of the generated noise. Noise is characterized by how its power spectral density varies with frequency. Common noise profiles are characterized by "power-law" noise, i.e., noise that follows a $1/f^{\beta}$ trend. In these simulations, we look at white Gaussian noise ($\beta = 0$) and colored noise ranging from violet to brown ($\beta = -2$ to 2).

The pulses are processed using both integration over the ideal integration pulse window for maximizing processed SNR and matched filter analysis. Once a full distribution is generated, it is fit to a Voigt distribution, and the fit temperature and its uncertainty are recorded. The process is repeated 1000 times, and the mean and standard deviation of temperatures and their uncertainties are recorded. If the goodness of fit falls below a threshold value, the "measurement" is recorded as failed.

The results in Fig. 3 use non-averaged single pulses per wavelength, whereas in Fig. 4, multiple pulses are averaged for each wavelength of a distribution to mimic data acquisition during an experiment.

## B. Analysis

Figure 3 compares the performance of the matched filter analysis to the integration method across different pulse SNRs, assuming white Gaussian noise and non-averaged single pulses at each wavelength. The performance of both methods was determined to not depend on the distribution width (i.e., temperature). Figure 3(a) shows how the relative uncertainties in the temperature fit vary with pulse SNR. The methods converge to <5% relative uncertainty at

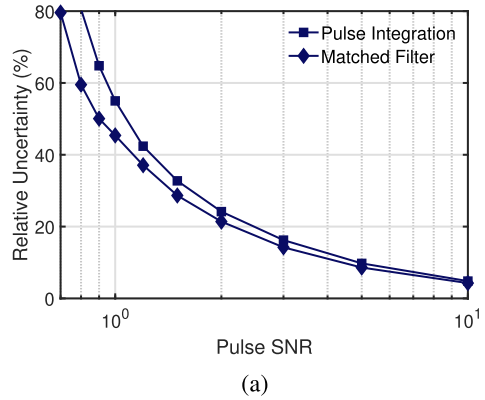


**FIG. 3.** (a) Uncertainty in temperature from VDF fits relative to the known temperature vs the pulse SNR of each pulse used to generate the distribution, and (b) the ratio of the standard deviations (matched filter compared to pulse integration) of the fitted temperatures and drift velocities. Generated from simulated 0.1 eV VDFs with one pulse per wavelength. The results did not vary by temperature.

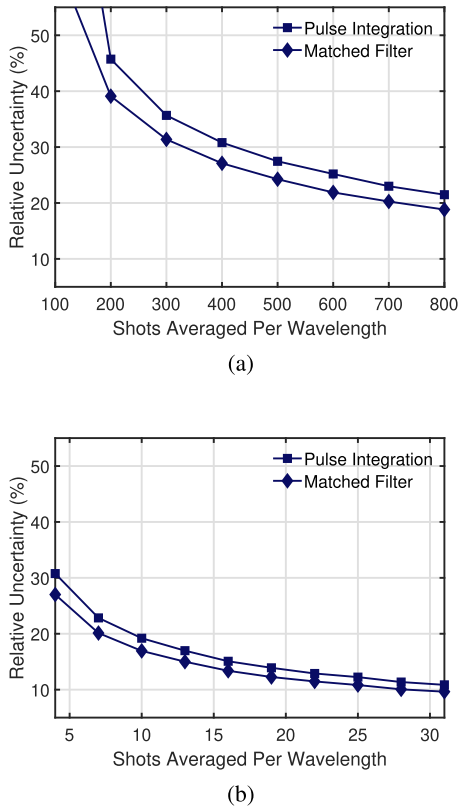


**FIG. 4.** The uncertainty in temperature obtained from fits to VDF relative to the known noise following a frequency response velocity distribution temperature (0.1 eV) vs the number of shots per wavelength in the distribution. Synthetic data generated for pulse SNRs of (a) 0.1 and (b) 1.0. Figures generated from simulated 0.1 eV distribution functions with variable pulses averaged per wavelength.

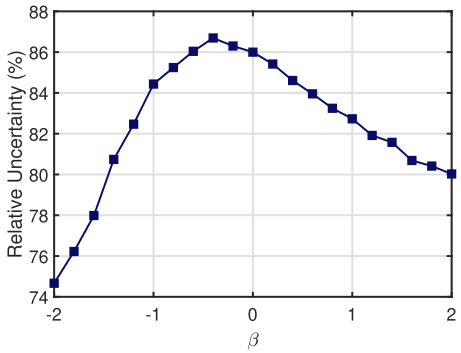


**FIG. 5.** The relative uncertainty (matched filter/pulse integration) of the temperature versus the color of the noise following a frequency response of $1/f^{\beta}$, with $\beta$ ranging from −2 (violet) to 2 (brown) noise.

a pulse SNR of >10. The uncertainties go to 100% around a pulse SNR of 0.8 for pulse integration and 0.7 for matched filter analysis. At that point, no fits yield reasonable values for the distribution function. These pulse SNR threshold values depend heavily on the number of averages used, as shown in Fig. 4. Shown in Fig. 3(b) is the ratio of the standard deviation of the distribution temperatures of each method ($\sigma_{MF,T}/\sigma_{Int.,T}$). Across investigated pulse SNR values, this ratio varies from around ~0.8 – 0.9, converging to ~0.9 at larger pulse SNR. In other words, the matched filter is consistently ~10 – 20% more precise.

Figure 4 shows the role of pulse averaging in the analysis process across both methods, comparing the relative uncertainty of the temperature values against the number of shots averaged per wavelength for pulse SNRs of 0.1 and 1. For both pulse SNR values, equivalent performance (the same relative uncertainty in the fit temperature) of the matched filter method compared to the integration method required ~20% fewer averages.

Changing the assumption of white Gaussian noise results in the relative performance of each method changing depending on the color of the noise. The pulse SNR is kept at 100. Figure 5 shows how varying the noise from blue to pink changes the ratio of relative uncertainty in the temperature fits for each method. White Gaussian noise ($\beta = -0.5$ to 0.5) provides the best relative performance for the pulse integration method, with a peak of 87%. Performance falls off steadily as the noise profile shifts into blue ($\beta = -1$) and pink ($\beta = 1$) noise and beyond. Therefore, the choice of white noise in the performance comparison of pulse integration to matched filter analysis was the best case scenario for pulse integration.

## IV. EXPERIMENTAL VALIDATION

### A. Methodology

A Quantel Q-scan pulsed dye laser, pumped by a Quantel Q-smart 850 Nd:YAG laser, was used for the LIF measurements reported here. The laser has a linewidth of ~1 GHz. For wavelength monitoring, ~15% of the light from within the laser cavity is split off and single mode fiber coupled to a HighFinesse WS6-200 wavelength meter with an absolute accuracy of 200 MHz. Approximately 2% of the laser is split off from the beamline for energy monitoring. The laser has a repetition rate of 10 Hz and a pulse width of 6 ns.

For proof-of-principle argon ion LIF measurements, the laser is injected into a steady-state helicon plasma source operating at a neutral pressure of 1.3 mTorr. The base pressure of the vacuum system is ~$10^{-8}$ Torr. External electromagnets generate an axial magnetic field of 720 G at the measurement location. Argon plasma is created with 500 W of rf power at a frequency of 13.56 MHz.

For this experiment, the $3d^2G_{9/2} \rightarrow 4p^2F^o_{7/2} \rightarrow 4s^2D_{5/2}$ LIF transition scheme for argon ions is used. Photons around the absorption wavelength of 611.6616 nm (vacuum) are injected radially into the plasma and are linearly polarized parallel to the axial magnetic field. The fluorescent 461.0858 nm (vacuum) photons are fiber coupled to a Hamamatsu H11526-20-NF fast PMT. A 1 nm bandpass filter centered at the fluorescent wavelength is placed between the fiber exit and the PMT detector face. The PMT signal is sent to a Lecroy HDO6054B digital oscilloscope with a time resolution of 0.1 ns and a bandwidth of 500 MHz.

Neutral density filters were inserted in the beam path to decrease the laser energy and control the pulse SNR. The laser wavelength was scanned through 21 pm around the central wavelength at 30 evenly spaced wavelength steps, with over 400 pulses recorded at each wavelength.

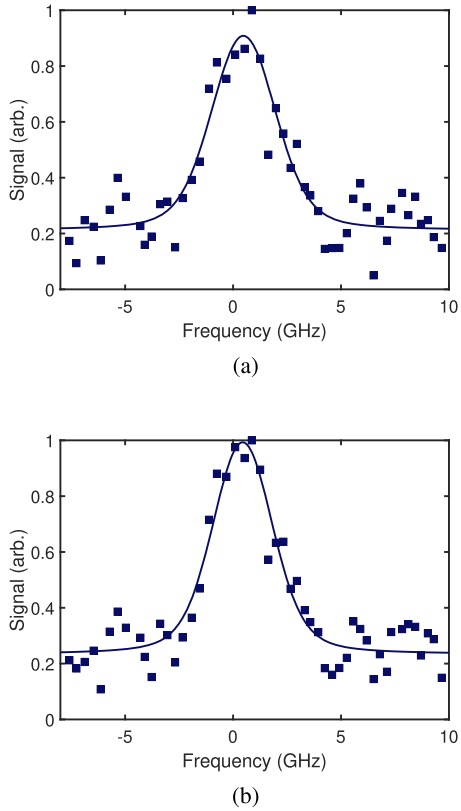


**FIG. 6.** Experimentally measured VDFs processed using (a) pulse integration and (b) matched filter analysis.

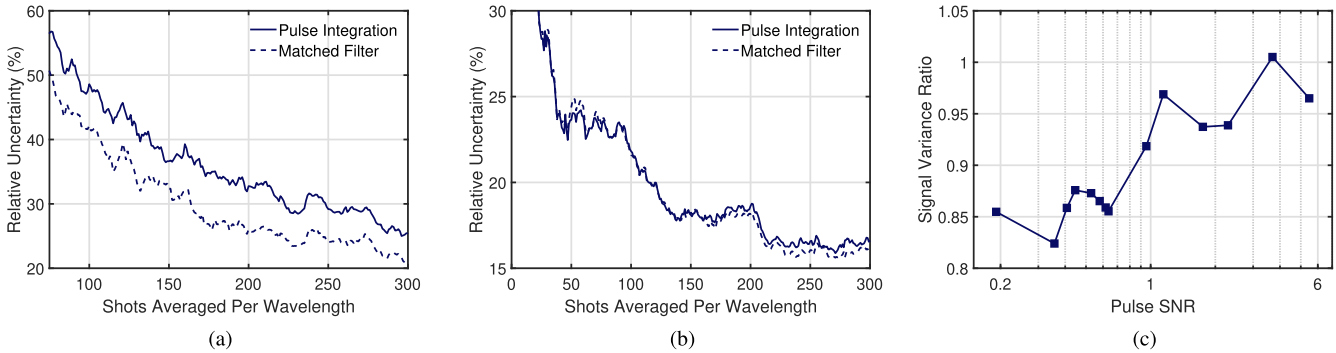


**FIG. 7.** Experimental uncertainty in temperature obtained from fits to VDF relative to the fully averaged velocity distribution temperature (~0.15 eV) vs the number of shots per wavelength in the distribution. Trends shown for pulse SNR of (a) 0.4 and (b) 3.7. In (c), the ratio (matched filter over pulse integration) of the processed signal variance is compared against the pulse SNR.

### B. Results

Distributions were measured at multiple laser energies, chosen to provide a range of pulse SNRs from ~0.2 to ~6. Figure 6 shows example distributions comparing the same set of data processed through pulse integration [Fig. 6(a)] and matched filter analysis [Fig. 6(b)]. These distributions were created from measurements in the 0.7 pulse SNR dataset. The variance in signal across the ion velocity distribution is clearly reduced with the matched filter method.

Figures 7(a) and 7(b) show how the relative uncertainty in the temperature for each method changes as a function of the number of shots averaged per wavelength for a small and a large pulse SNR, respectively. The relative performance of each method remains approximately consistent across averages for a given pulse SNR; however, the relative performance clearly differs across different pulse SNRs.

Figure 7(c) shows how the relative variance between matched filtering and pulse integration changes with respect to pulse SNR. For each unique pulse SNR, each laser pulse time series is analyzed using the matched filter or integration method at the peak laser wavelength (the wavelength corresponding to the peak of the particle distribution). More than 400 separate instances of signal extracted from the pulse time series are produced for each approach. The respective (matched filter or integration) data points are then normalized to the respective mean of each group and the standard deviation of each group, is computed. Shown in Fig. 7(c) is the ratio of the standard deviation from the matched filter approach and the integrated approach (matched filter over integration) as a function of pulse SNR. Values of this ratio less than one indicate the variance in signal derived from the integration technique is larger than the variance in signal derived from the matched filter approach. For pulse SNRs below one, the matched filter technique detects signals with ~15% less variance than the integration approach. For pulse SNR >1, the signal variances converge, with the matched filter signal having ~5% less variance than pulse integration.

For the tested pulse SNRs between 0.36 and 0.95, the performance of the matched filter analysis of the measurements over pulse integration analysis is similar to the simulated results, showing an ~10%–20% improvement in relative fit uncertainty. At a pulse SNR of 0.2 (the lowest pulse SNR attempted), neither method is able to reliably extract sufficient signal to fit good distributions within 600 laser pulses.

## V. CONCLUSIONS

The simulated results were validated by experiment and highlighted the increased sensitivity of signal detection using a matched filter processing technique rather than the traditional pulse integration method. Simulation results show that in ideal conditions with pure Gaussian white noise added to a signal, the matched filter processing technique statistically achieves ~14% lower relative uncertainty and ~10 to 20% better precision in the temperature measurements than pulse integration. Real world experiments often follow a "pink noise" $1/f$ power spectrum, where simulation results show the matched filter statistically achieves a relative uncertainty of ~17% lower than pulse integration. Experimental results showed a range of ~10 to 20% lower relative uncertainty in the temperature fits for the matched filter analysis. The fit uncertainties of these experimental results fall within two standard deviations of the expected fit uncertainty based on simulations with similar parameters. Despite typically higher uncertainty in the fit, temperature measurements for pulse integration analysis typically follow those of matched filter analysis closely until pulse SNRs fall below 0.7. Eventually, the two methods converge with higher pulse averages.

Below a pulse SNR of 0.2, reliable ion temperature measurements were not achieved, but the general structure of the VDF did emerge from the noise. It is possible that further averaging may result in a successful measurement. For very small pulse SNR, the limited bit resolution of the oscilloscope is expected to limit the ability of either method, regardless of averaging.

The matched filter method effectively reduces experimental time by up to 25% compared to pulse integration. For PHASMA with a discharge cadence of one shot per 30 s, this reduces the time needed for a single VDF measurement by hours. Even in situations where experimental time is not a significant consideration, the matched filter still provides more precise results. Matched filtering analysis is effective for pulsed LIF and is a suitable method for distribution measurements, especially for small pulse SNR.

## ACKNOWLEDGMENTS

This work was supported by the WVU Center for KINETIC Plasma Physics and the Nat. Sci. Foundation Grant No. PHY-190211.

## AUTHOR DECLARATIONS

### Conflict of Interest

The authors have no conflicts to disclose.

### Author Contributions

**T. J. Gilbert**: Conceptualization (supporting); Data curation (lead); Formal analysis (lead); Investigation (lead); Methodology (lead); Writing – original draft (lead); Writing – review & editing (equal). **T. E. Steinberger**: Conceptualization (supporting); Data curation (supporting); Methodology (supporting); Writing – review & editing (equal). **E. E. Scime**: Conceptualization (lead); Funding acquisition (lead); Project administration (lead); Writing – review & editing (equal).

## DATA AVAILABILITY

The data that support the findings of this study are available from the corresponding author upon reasonable request.

## REFERENCES

[1]P. Shi, K. Huang, Q. Lu, and X. Sun, Plasma Phys. Controlled Fusion **61**, 125010 (2019).
[2]P. Shi, P. Srivastav, C. Beatty, R. S. Nirwan, and E. E. Scime, Rev. Sci. Instrum. **92**, 033102 (2021).
[3]T. D. Phan, J. P. Eastwood, M. A. Shay, J. F. Drake, B. U. Ö. Sonnerup, M. Fujimoto, P. A. Cassak, M. Øieroset, J. L. Burch, R. B. Torbert, A. C. Rager, J. C. Dorelli, D. J. Gershman, C. Pollock, P. S. Pyakurel, C. C. Haggerty, Y. Khotyaintsev, B. Lavraud, Y. Saito, M. Oka, R. E. Ergun, A. Retino, O. Le Contel, M. R. Argall, B. L. Giles, T. E. Moore, F. D. Wilder, R. J. Strangeway, C. T. Russell, P. A. Lindqvist, and W. Magnes, Nature **557**, 202 (2018).
[4]M. Yamada, J. Yoo, J. Jara-Almonte, H. Ji, R. M. Kulsrud, and C. E. Myers, Nat. Commun. **5**, 4774 (2014).
[5]J. L. Kline, E. E. Scime, R. F. Boivin, A. M. Keesee, X. Sun, and V. S. Mikhailenko, Phys. Rev. Lett. **88**, 195002 (2002).
[6]G. Turin, IEEE Trans. Inf. Theory **6**, 311 (1960).
[7]E. Voigtman, Appl. Spectrosc. **45**, 237 (1991).
[8]Z. Feizhou and L. Shanghe, IEEE Trans. Electromagn. Compat. **44**, 595 (2002).
[9]S. E. Bialkowski, Appl. Spectrosc. **42**, 807 (1988).
[10]W. Demtröder, *Laser Spectroscopy 1: Basic Principles* (Springer Berlin, Heidelberg, 2014), Vol. 1.
[11]M. C. Paul and E. E. Scime, Rev. Sci. Instrum. **92**, 043532 (2021).
[12]S. M. Abrarov and B. M. Quine, "The voigt/complex error function," https://www.mathworks.com/matlabcentral/fileexchange/47801-the-voigt-complex-error-function-second-version, MATLAB Central Filed Exchange, 2016, Online; accessed 2021.
[13]N. Vitanov, B. Shore, L. Yatsenko, K. Bohmer, T. Halfmann, T. Rickes, and K. Bergmann, Opt. Commun. **199**, 117 (2001).
[14]M. J. Goeckner, J. Goree, and T. E. Sheridan, Rev. Sci. Instrum. **64**, 996 (1993).